



HAL
open science

Analytical Design of a Finite Input Inductance 34.5 MHz Class E Inverter for Wireless Power Transfer

Matthieu Beley, Mohamed El-Khattabi, Loris Pace, Arnaud Bréard

► **To cite this version:**

Matthieu Beley, Mohamed El-Khattabi, Loris Pace, Arnaud Bréard. Analytical Design of a Finite Input Inductance 34.5 MHz Class E Inverter for Wireless Power Transfer. International Conference on Integrated Power Electronics Systems, Power Engineering Society VDE ETG, Mar 2024, Düsseldorf, Germany. hal-04483567

HAL Id: hal-04483567

<https://hal.science/hal-04483567v1>

Submitted on 29 Feb 2024

HAL is a multi-disciplinary open access archive for the deposit and dissemination of scientific research documents, whether they are published or not. The documents may come from teaching and research institutions in France or abroad, or from public or private research centers.

L'archive ouverte pluridisciplinaire **HAL**, est destinée au dépôt et à la diffusion de documents scientifiques de niveau recherche, publiés ou non, émanant des établissements d'enseignement et de recherche français ou étrangers, des laboratoires publics ou privés.

Analytical Design of a Finite Input Inductance 34.5 MHz Class E Inverter for Wireless Power Transfer

Matthieu BELEY ⁽¹⁾, Mohamed EL-KHATTABI ⁽²⁾, Loris PACE ⁽¹⁾, Arnaud BREARD ⁽¹⁾

⁽¹⁾ Ecole Centrale de Lyon, INSA Lyon, Université Claude Bernard Lyon 1, CNRS, Ampère, UMR5005, 69130 Ecully, France

⁽²⁾ CNRS, INSA Lyon, Université Claude Bernard Lyon 1, Ecole Centrale de Lyon, Ampère, UMR5005, 69130 Ecully, France

Abstract

The demand for lighter and more compact power converters is an opportunity for reducing their costs and environmental footprint. This work proposes an analytical method for the design of a finite input inductance class E inverter which is a fundamental topology in Very High Frequency (VHF – 30MHz to 300MHz) power converters. Validation of the method is performed through the fabrication of a 100W inverter operating at 34.5MHz, for Wireless Power Transfer (WPT) through Magnetic Resonant Coupling (MRC). An accurate model based on Electro-Magnetic (EM) simulation and high frequency (HF) characterization of passive components is presented.

1 Introduction

The research oriented toward VHF power conversion is gaining interest in the global context of electrification [1]. The very high switching frequency of such converters allow to shrink their size for a given power, hence achieving higher power density. The incorporation of parasitic components into the structure allow shorter bills of material, hence reducing the heterogeneity of the system. Applications of VHF converters cover for example Wireless Power Transfer (WPT) [2, 3], compact LED drivers [4], plasma etching [5] or satellite propulsion [6].

When it comes to high frequencies, typical topologies consisting of hard-switched transistors cannot be used any longer, due to the impact of switching losses. Furthermore, it becomes extremely difficult to drive high-side switches, and to guarantee the implementation of dead times. To counteract the frequency-dependent losses, ground referenced single switch resonant topologies, originated from Radiofrequency applications, are widely used in VHF power conversion [1]. Zero Voltage Switching (ZVS) and Zero Derivative Voltage Switching (ZDVS) are achieved within the switch at turn-on [1]. Current in the capacitor in parallel with the switch (including the parasitic C_{OSS}) is equal to zero at turn-on with ZDVS. To prevent frequency-dependent losses in the magnetic core of inductors (Eddy currents and hysteresis) air-core technology is mainly used, either printed on the board or wire-wound. Air-core inductors still suffer from skin and proximity effects.

The class E inverter is a widely used topology in VHF power converters [1]. Its main advantages are its relatively simple design and the unique ground-referenced switch, whereas the drawbacks are the voltage stress upon the switch and the fact that performances are lowered while load is changing [7]. It can be for example operated as the first stage of a VHF DC-DC power conversion system, as enlightened in **Figure 1** [1]. Compared to a traditional class E inverter where the input inductance has a high enough value to keep the input current constant [8], the input inductance in the Finite Input Inductance (FII) class E inverter resonates with the capacitor in parallel

with the switch. This improves dynamic of the inverter, which could be beneficial for control (not considered in this work). Power density and robustness against load variation are improved as well [9].

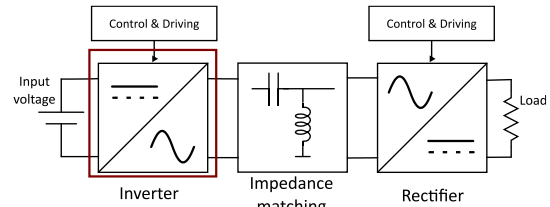


Figure 1 Typical VHF DC-DC converter schematic

Ideal operation of FII class E inverter is first analysed in [9], and several papers give design method considering non-idealities such as non zero switch resistance or finite quality factor of the output filter [10]. An analytical design method allowing arbitrary value for the duty cycle is presented in [10] and [11]. The method remains long and complex, and only validated in simulation. This article aims to propose a reproducible analytical design method for a FII class E inverter. An operating point can be selected based on design criteria related to power converters, such as voltage stress applied on the switch or minimal value for passive components. The method is validated through the fabrication of a FII class E inverter prototype operating at 34.5MHz for WPT application. A model of the inverter based on High Frequency (HF) characterization is developed. The model also considers the parasitic impedances brought by the Printed Circuit Board, thanks to an Electro-Magnetic (EM) simulation conducted in Advanced Design System®. At the author's knowledge, there is no work in the literature detailing and validating the analytical design of FII class E inverter applied to VHF power conversion.

Section 2 provides the analytical design method for a FII class E inverter. The proposed method is then applied to a 100W 34.5MHz class E inverter for WPT application in Section 3. The modelling of the system is detailed in Section 4. Then experimental waveforms of the prototype are measured and compared to the proposed model in Section 5. Conclusion and future work are given in Section 6.

2 Analytical design

The FII class E inverter topology is given on **Figure 2**. Its operation and the derivation of its analytical expressions have been discussed in the literature [10]. The transistor is driven at the switching frequency f by means of an external gate driver, at duty cycle D . Period T is normalized to 2π and angle $\theta = \omega t$ is introduced. The LC series filter ($L_s - C_s$) resonate at f whereas the input LC circuit ($L_p - C_p$) resonates at qf . The parameters D and q are the two degrees of freedom in the analytical design, and are defined as (1):

$$D = \frac{\theta_{ON}}{2\pi} \text{ and } q = \frac{1}{\omega\sqrt{L_p C_p}} \quad (1)$$

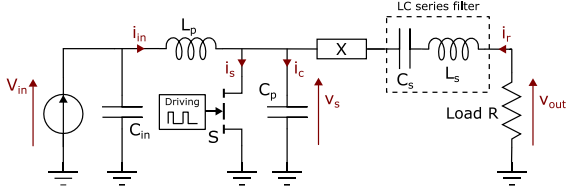


Figure 2 FII class E inverter schematic

Theoretical waveforms of current i_s and voltage v_s within the switch, and output voltage v_{out} are given on **Figure 3**. The switch is closed during $\theta_{ON} = 2\pi D$ and open during $\theta_{OFF} = 2\pi(1 - D)$. Ideal operation (ZVS and ZDVS) is achieved within the switch.

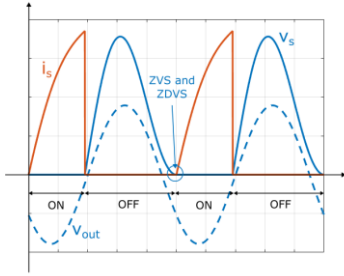


Figure 3 Ideal waveforms of the class E inverter

The analytical design is based on following assumptions:

1. The power switch is ideal (instantaneous switching, zero ON-resistance and infinite OFF-resistance).
2. The loaded quality factor Q_L of the output filter is high enough such that the resonant current i_r is sinusoidal and is defined as (2):

$$i_r(\theta) = I_r \sin(\theta + \phi) \quad (2)$$

With I_r the magnitude and ϕ the initial phase shift.

3. The input voltage V_{in} is DC.
4. The load R is the only component to consume active power, such that $P_{in} = P_{out}$.
5. The shunt capacitance C_p is voltage independent.

In this article, the design inputs are V_{in} , R and f . The objective of the design stage is to obtain ideal values for the electrical parameters (P , C_p , L_p , C_s , L_s) and closed-form expressions for the current/voltage waveforms. The designer can explore the design space while complying with design constraints to find an operating point. In theory, once q and D are set, the solution which guarantees class E optimal operation is unique. To summarize, the design flow is depicted in **Figure 4** and detailed in this section. Ratio p is introduced for convenience (3):

$$p = \frac{\omega L_p I_r}{V_{in}} \quad (3)$$

The analysis is done for the two configurations: S open and S closed.

- When S is closed ($\theta < 2\pi D$):

No current flows into C_p and $i_{in} + i_r$ flows into S . With regard to the relation between current and voltage within inductors, the following expressions (4-5) are derived:

$$i_s(\theta) = I_r \left(\frac{\theta}{p} + \sin(\theta + \phi) - \sin(\phi) \right) \quad (4)$$

$$v_s(\theta) = 0 \quad (5)$$

- When S is open ($\theta \geq 2\pi D$)

No current flows into S , current $i_{in} + i_r$ flows into C_p , and i_{in} flows into L_p . With regard to the relation between current and voltage within capacitors and inductors, a linear non-homogeneous second order ODE can be written for v_s (6):

$$L_p C_p \omega^2 \frac{d^2 v_s(\theta)}{d\theta^2} + v_s(\theta) = V_{in}(1 + p \cos(\theta + \phi)) \quad (6)$$

Solving this ODE, v_s can be written as (7):

$$v_s(\theta) = V_{in} \left(1 + k_1 \cos(q\theta) + k_2 \sin(q\theta) + \frac{q^2 p}{q^2 - 1} \cos(\theta + \phi) \right) \quad (7)$$

Where $k_1(p, \phi, q, D)$ and $k_2(p, \phi, q, D)$ are two constants to be determined with conditions relative to ZVS (8) and

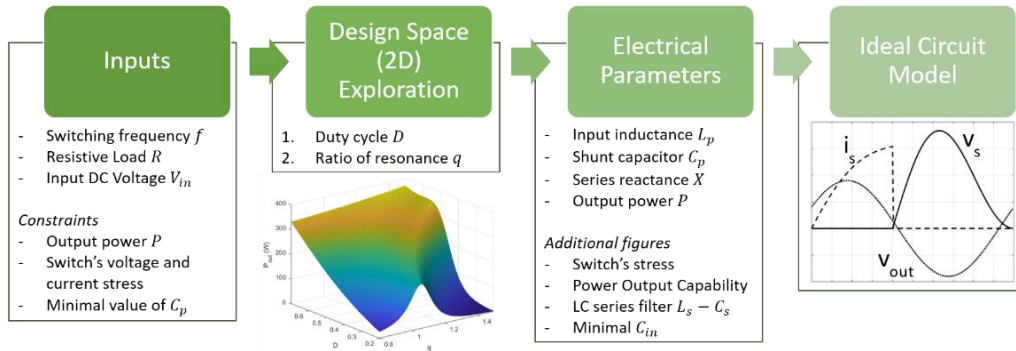


Figure 4 Design flow of the FII class E inverter, with f , R and V_{in} as inputs

ZDVS (9) of the switch:

$$v_s(2\pi) = 0 \quad (8)$$

$$\frac{dv_s(\theta = 2\pi)}{d\theta} = 0 \quad (9)$$

Parameters $p(q, D)$ and $\phi(q, D)$ can be determined with regard to the following boundary conditions (10-11):

$$v_s(2\pi D) = 0 \quad (10)$$

$$i_c(2\pi D) = i_s(2\pi D) \quad (11)$$

Parameters k_1, k_2, p and ϕ only depends on q and D and their expressions are given in the Appendix.

Current gain $g_x = \frac{\langle i_s \rangle_{>2\pi}}{I_r}$ of the inverter under the small ripple approximation is calculated with (12) [11]:

$$g_x(q, D) = \frac{\pi D^2}{p} - D \sin \phi + \frac{\cos \phi}{2\pi} - \frac{\cos(2\pi D + \phi)}{2\pi} \quad (12)$$

Equating P_{out} and P_{in} leads to the expression (13):

$$\frac{RI_r^2}{2} = V_{in} \langle i_{in} \rangle_{>2\pi} \quad (13)$$

The expressions (14-15) are assessed:

$$\langle i_{in} \rangle_{>2\pi} = \langle i_s \rangle_{>2\pi} + \langle i_c \rangle_{>2\pi} - \langle i_r \rangle_{>2\pi} = \langle i_s \rangle_{>2\pi} \quad (14)$$

$$g_x = \frac{RI_r}{2V_{in}} \quad (15)$$

The following expressions (16-18) giving P, L_p, C_p and R_{in} are then derived from (1, 3, 13, 15):

$$P = \frac{2g_x^2 V_{in}^2}{R} \quad (16)$$

$$L_p = \frac{pV_{in}}{\omega I_r} = \frac{pR}{2g_x \omega} \quad (17)$$

$$C_p = \frac{1}{q^2 \omega^2 L_p} \quad (18)$$

V_{out} magnitude and input resistance R_{in} of the inverter are provided by (19-20):

$$V_{out} = RI_r = 2g_x V_{in} \quad (19)$$

$$R_{in} = \frac{V_{in}}{\langle i_{in} \rangle_{>2\pi}} = \frac{R}{2g_x^2} \quad (20)$$

The LC series filter ($L_0 - C_0$) which is tuned to frequency f is designed in regard with the system of equations (21):

$$\begin{cases} Q_L = \frac{1}{R} \sqrt{\frac{L_0}{C_0}} \\ \omega = \frac{1}{\sqrt{L_0 C_0}} \end{cases} \quad (21)$$

With Q_L chosen sufficiently high (a practical range is between 5 and 15 [7]) to filter out high-order harmonics in current i_r .

The actual LC series filter ($L_s - C_s$) is detuned to a slightly different frequency, in order to induce the correct phase shift ϕ and thus ideal operation of the class E inverter. A First Harmonic Approximation (FHA) is considered to design the series reactance X leading to this correct phase shift. It is assumed that the power is only transmitted from switch's node to load at frequency f due to the sinusoidal

current i_r . At frequency f , the output branch of the class E inverter can be represented as in **Figure 5**.

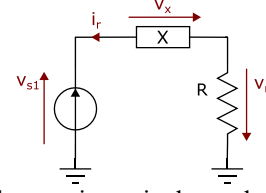


Figure 5 First harmonic equivalent schematic of the output branch of the FII class E inverter, at frequency f

The first harmonic of $v_s(\theta)$ can be written as (22):

$$v_{s1}(\theta) = V_r \sin(\theta + \phi) + V_x \cos(\theta + \phi) \quad (22)$$

Where the components V_r and V_x are respectively in phase and quadrature with i_r , and are calculated with (23-24):

$$V_r = \frac{1}{\pi} \int_0^{2\pi} v_s(\theta) \sin(\theta + \phi) d\theta \quad (23)$$

$$V_x = \frac{1}{\pi} \int_0^{2\pi} v_s(\theta) \cos(\theta + \phi) d\theta \quad (24)$$

The analytical expressions of V_r and V_x are given in the Appendix. X is given by (25):

$$X = R \frac{V_x}{V_r} \quad (25)$$

Reactance X can be either positive or negative. L_s and C_s are finally given by (26-27):

$$\text{If } X > 0 : L_s = L_0 + \frac{X}{\omega} \text{ and } C_s = C_0 \quad (26)$$

$$\text{If } X < 0 : C_s = \frac{C_0}{1 + C_0 X \omega} \text{ and } L_s = L_0 \quad (27)$$

Switch voltage and current stresses can be calculated with the following empirical expressions (28-29) [11]:

$$V_{smax} = \frac{1.7613 + 0.05q}{(1 - D)} V_{in} \quad (28)$$

$$I_{srms} = \frac{V_{in} g_x}{R} \cdot \frac{f_1}{f_2} \quad (29)$$

Parameters f_1 and f_2 are given in the Appendix.

Since parameters ϕ, p and X and the values of passive components only depend on q and D , it is possible to explore freely the 2D design space, varying the values of q and D . Preliminary ideal design of the class E inverter is then achieved by finding an operating point complying with design constraints.

3 Design of the class E prototype

3.1 WPT system

WPT to the RF load is performed through the inductive coupling of two open-type resonant coils [3]. Both primary and secondary resonant coils are made of two coils printed on each side of the PCB (dielectric Flame Retardant 4 (FR4), thickness $t = 3.2\text{mm}$) and capacitively coupled. The load seen by the inverter is the system consti-

tuted by the resonant coils and the RF load. **Figure 6** shows the synoptic of the resonant coils within the WPT system, as well as the electrical schematic [3].

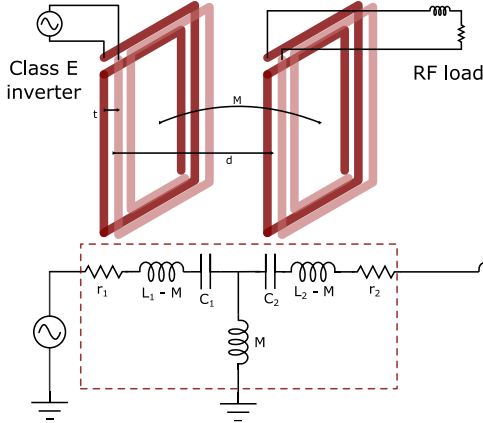


Figure 6 Synoptic and schematic of the WPT system

The RF load is the parallel connection of four 50Ω RF load Anaren C150N50Z4, and Equivalent Series Inductance (ESL L_L) of the interconnections have been measured to 1nH. L_1 , C_1 , L_2 and C_2 are the electrical parameters of both resonant coils, and their Equivalent Series Resistance (ESR) is denoted r_1 and r_2 . M is the mutual inductance between them, which is connected to the coefficient of coupling k with the expression (34):

$$M = k\sqrt{L_1 L_2} \quad (34)$$

Parasitic impedances r_1 , r_2 and L_L can be neglected at first, and the impedance of the WPT load $Z_{WPT-load}$, which is denoted R , can be expressed analytically. As the two resonant coils are built such that their resonant frequency equals f , R is given by (35) [3]:

$$R = j\left(\omega L_1 - \frac{1}{\omega C_1}\right) + \frac{(\omega M)^2}{R_{RF} + j\left(\omega L_2 - \frac{1}{\omega C_2}\right)} = \frac{(\omega M)^2}{R_{RF}} \quad (35)$$

$$= k^2 \frac{\omega^2 L_1 L_2}{R_{RF}}$$

$Z_{WPT-load}$ is purely resistive, and depends strongly on k , hence on d . Therefore, a certain distance ($d = 8cm$) has been chosen experimentally for this prototype, in order to keep the impedance constant ($R = 5\Omega$) and thus maintain the optimal operation of the class E inverter. Future works is planned in order to design a VHF class E inverter more robust in front of load variations [12]. Section 4.1 gives the electrical model of the WPT load.

3.2 Analytical method testing

The GaN HEMT GS61004B (100V, 38A, 16mΩ) from GaN Systems is selected for the class E inverter design, in regard with its good characteristics at high switching frequencies. Low R_{DSon} (16mΩ), low parasitic capacitances ($C_{iss} = 260pF$ and $C_{oss} = 110pF$ at $V_{DS} = 50V$) and low packaging inductances are beneficial for an usage in VHF power converters [13]. The inverter is then designed in accordance with requirements given in **Table 1**.

Table 1 Design requirements

Figure	Value
DC input voltage V_{in}	24 V
Load R	5 Ω
Output power P	[95;105] W
Switching frequency f	34.5 MHz
Maximal drain-source voltage $V_{s,max}$	80 V
Minimal loaded quality factor Q_L	7
Minimal shunt capacitor C_p	500 pF
Input inductance L_p	[22;500] nH

f and R values are chosen in accordance with the WPT load. $V_{s,max}$ is chosen below the breakdown voltage of the transistor. Q_L has to be high enough to validate the design assumptions. C_p has to be high enough to overcome the non-linearity of the transistor's C_{oss} and therefore validate design assumption.

The theoretical range of variation of D is between 0 and 1. Nevertheless, D should not be too much distant from 0.5 in the VHF range, as rise and fall times and hence narrowness of pulses for v_{GS} are limited by the gate driver. A range between 0.3 and 0.9 could be chosen [14], but since the maximum drain-source voltage v_s has to be lower than 80 V, high values of duty cycle are forbidden. For these reasons, possible variation range of D is between 0.3 and 0.6. The possible range of variation of q is between 0 (case where L_p is infinite [8]) and 2 (values higher than 2 leads to phase-shift ϕ higher than $\frac{\pi}{2}$).

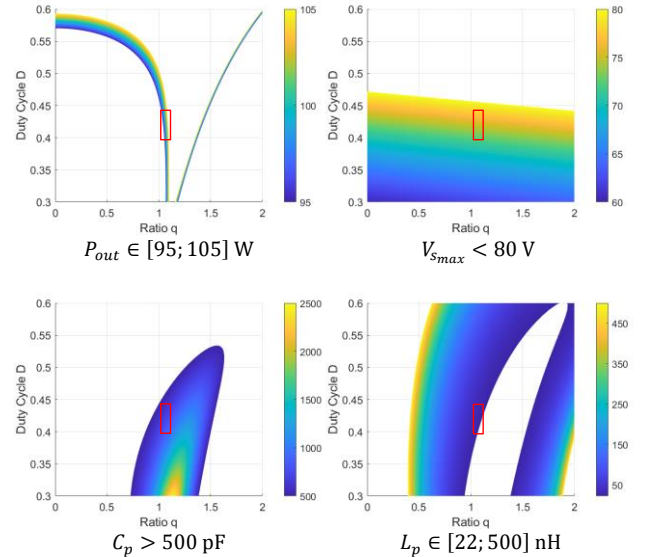


Figure 7 2D (q , D) design exploration with constraints

2D design space exploration complying with the previously stated requirements lead to the charts in **Figure 7**. The operating point has to be within the coloured areas. In regard with the previous charts, parameters q and D are within intervals:

$$q \in [1.05 - 1.08]$$

$$D \in [40\% - 44\%]$$

Therefore, the following operating point has been selected: $q = 1.075$ and $D = 41\%$. Q_L is chosen to be equal to 9.1, which provide values for the LC series filter components close to commercial standards and guarantees a sufficient filtering of the i_r harmonics. This leads to the design solution contained in **Table 2**.

Table 2 Chosen design solution ($q = 1.075$, $D = 41\%$)

L_p	23.4 nH	L_s	223 nH
C_p	788 pF	C_s	101 pF
P_{out}	101 W	$V_{out_{rms}}$	22.5 V
$V_{s_{max}}$	74 V	$I_{s_{rms}}$	4.6 A

3.3 Final design

The final design of the inverter is summarized in **Table 3**.

Table 3 Technological design

L_p	22 nH – Coilcraft 1212VS-22NMED
C_p	560 pF – C0G KEMET C0805C561JCGACTU
C_{in}	100 nF – X7R Wurth Elektronik 885342211002
L_s	220 nH – Coilcraft 2222SQ-221JEC
C_s	100 pF – C0G KEMET C0805C101FCGACTU
GaN HEMT	GaN Systems GS61004B
Gate driver	Texas Instrument LMG1020

Values of passive components are chosen close to the ideal values. C0G dielectric Multi-Layer Ceramic Capacitor (MLCC) are chosen for the resonant capacitors, and wire-wound air core inductors are selected, based on available values. A 100nF capacitor is placed at the input of the inverter to limit ripple on v_{in} . X7R dielectric is chosen since the capacitance value is not critical. LMG1020 is chosen to drive the gate of the GaN HEMT, in regard with its low rise and fall times ($< 400ps$ for a 0Ω resistor in series with a 100pF load). The non-linear output capacitance C_{OSS} of the GaN HEMT is taken into account by removing approximately 200pF to the ideal value of C_p .

4 Modelling

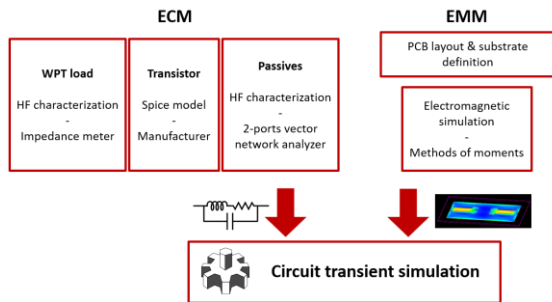


Figure 8 Flow of the system modelling

A model of the global system (class E inverter, Resonant coils, and RF Load) is introduced in this section. **Figure 8** depicts the modelling flow, from the equivalent circuit models (ECM) and electromagnetic models (EMM) to the circuit transient simulation of the system, conducted in the Advanced Design System® (ADS) environment. The SPICE model from the manufacturer is used for the GaN

HEMT and passive voltage probes are modelled by their input capacitance (9.5 pF).

The gate driver is modelled as a push-pull stage in series with gate resistors (see **Figure 9**) and values are extracted from the manufacturer's model.

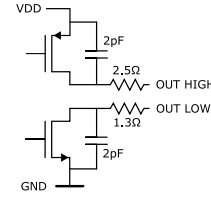


Figure 9 Electrical model of the gate driver LMG1020

Derivation of the ECM, through HF characterization, and EM modelling of the PCB are detailed in the three sections below.

4.1 ECM of the WPT load

The WPT load described in Section 3 is characterized with the impedance analyser Keysight E4991B, and is loaded by the 12.5Ω RF load. **Figure 10** gives the impedance measurement and its modelling with the RLC ECM valid at the operating frequency $f = 34.5MHz$. As power is transferred mainly at the first harmonic, this model is considered sufficient for the modelling of the full system.

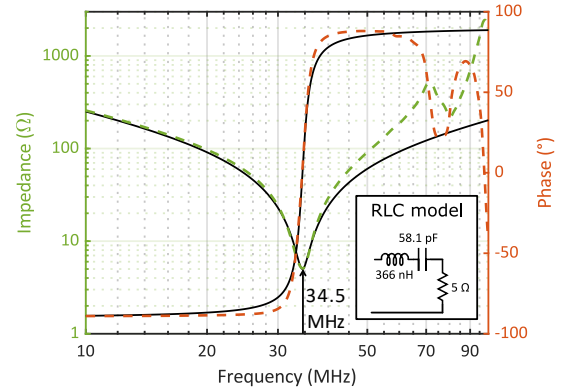


Figure 10 Measure of impedance magnitude of the WPT load, loaded by $R_{load} = 12.5\Omega$

4.2 ECM of passive components

In order to obtain the ECM of the passive components, a HF characterization is performed. ECM is obtained through 2-ports S parameters measurement on a Vector Network Analyzer. This allows the extraction of an ECM valid on a wide frequency range [15].

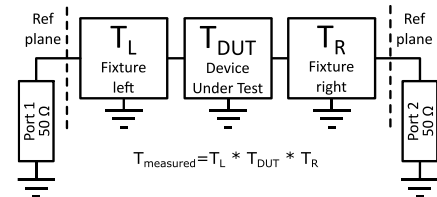


Figure 11 Cascading of transfer (T) parameters matrices

For that purpose, characterization PCBs are fabricated, and S parameters are measured with and without DUT in order to get the single effect of the fixture (Coaxial con-

nectors and PCB traces). De-embedding of fixture is then performed through T-matrix calculation, as shown in **Figure 11**.

Once de-embedding is done, Z/Y parameters of the two-port network DUT are calculated [15]. Depending on the DUT arrangement (Shunt or Serie), a PI or T equivalent network of the DUT is derived, as shown in **Figure 12**.

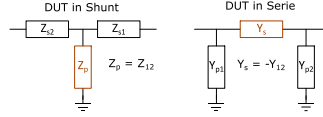


Figure 12 Equivalent circuit model of Device Under Test (DUT) placed in Shunt and in Series between the 2 ports

Capacitors C_p and C_s have been characterized in Series-through configuration ($Z_C > 50 \Omega$ when extracting capacitance value), whereas inductors L_p and L_s in Shunt-through configuration ($Z_L < 50 \Omega$ when extracting inductance value). **Figure 13** gives the impedance magnitude of components C_p , C_s , L_p and L_s after de-embedding. The model is shown in black dashed line for comparison.

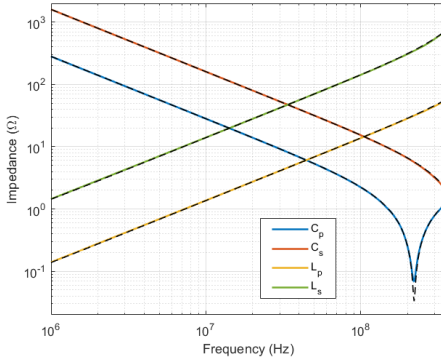
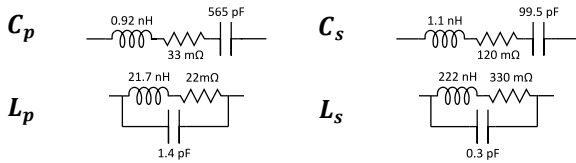


Figure 13 Impedance magnitude of components L_p , C_p , L_s and C_s with their models

An ECM valid at $f = 34.5\text{MHz}$ is derived from the measured real and imaginary part of the impedance. **Table 4** summarizes the four ECM considered for the passive components of the class E inverter.

Table 4 ECM of components C_p , L_p , C_s and L_s



4.3 EMM of the PCB

The inverter circuit is printed on FR4 substrate (0.4 mm thickness) with two layers copper (35 μm thickness). The bottom layer is referenced to ground, except for the traces of inductor L_s , placed on the bottom side to reduce couplings with L_p . PCB layout is represented in **Figure 14**.

This layout has been imported within the electromagnetic simulation (EM) environment ADS, and the substrate parameters has been defined. Ports have been placed onto the PCB, for each connection with external components. S parameters, up to 1 GHz, has been afterwards obtained

thanks to the EM simulation (RF Method of Moments, 20 cells/wavelength). An EM model of the PCB is then created and components (passive and the GaN HEMT) can be connected onto it, in a circuit transient simulation. Hence, parasitic impedances brought by the PCB are taken into account in the general model.

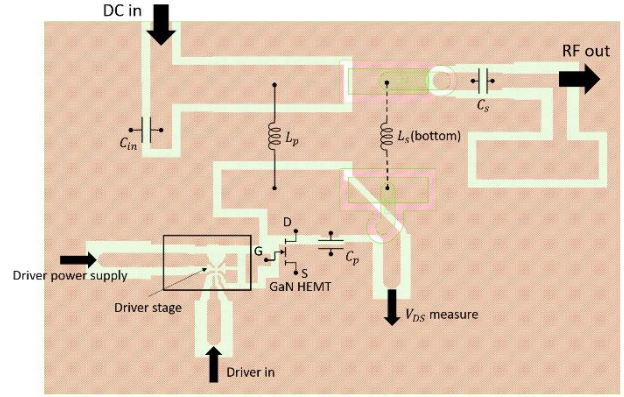


Figure 14 Class E inverter PCB and components layout

5 Experimental validation

The prototype is characterized and voltage waveforms are probed using passive voltage probe ProbeMaster 5900 Series (bandwidth 500MHz) and oscilloscope Tektronix MSO64. The square signal ($f = 34.5\text{MHz}$ and $D = 38\%$) is generated by the arbitrary waveform generator Tektronix AFG 3252. D is slightly adjusted in order to obtain an effective duty cycle of 41% when probing gate-source voltage v_{GS} .

A prototype of the previously described class E inverter is manufactured, as well as both resonant coils and the RF load. A photograph of the inverter prototype is presented in **Figure 15**.

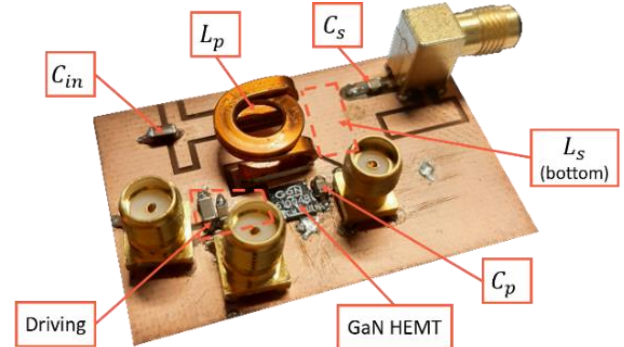


Figure 15 Photograph of the FII class E inverter board

The tests have been carried out at nominal input voltage in pulse mode, in order to prevent self heating. Voltage waveforms measured across the GaN HEMT are given in **Figure 16**. Waveforms obtained through the modelling process described in Section 4 are shown in dashed lines for comparison, and are taken at the external terminals of the GaN HEMT circuit model.

A good accordance is observed between model and measurements. Inductance of the commutation loop generates high frequency (around 540MHz) oscillations on v_s . As

v_{GS} is not exactly probed at switch's terminals, oscillations appear due to the common source inductance.

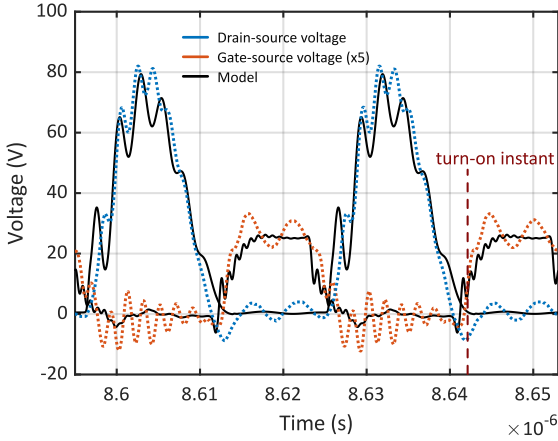


Figure 16 Probing of v_s and v_{GS} (multiplied by 5) and comparison with the model

Figure 17 gives the waveforms measurement of input and output voltages. The voltage probe adds a non-negligible capacitance, which modifies the impedance of the output branch constituted by the LC series filter and the load. third order harmonic appears in the modelled v_{out} waveforms. As the WPT load model is valid only up to fundamental frequency, frequency content of v_{out} is not well predicted but this does not impact the transmitted power.

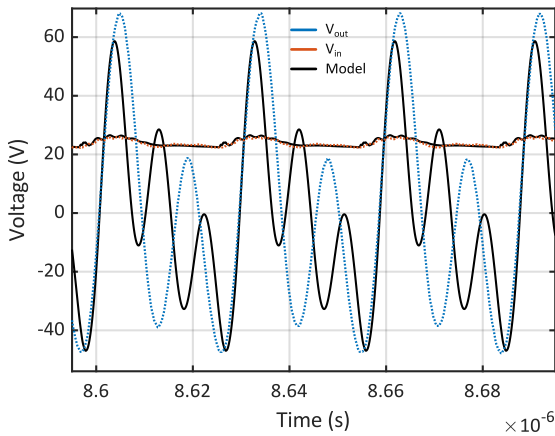


Figure 17 Probing of v_{out} and v_{in} and comparison with the model

Output power given by the model reaches 61W, for an input power of 79W ($\eta = 77\%$). The difference compared to the output power obtained with the ideal model comes from parasitic impedances modifying the input impedance of the converter, and the detuning of the output filter. Considering that the power is transmitted only at first harmonic, as (36):

$$P_{out} = \frac{V_{out_1}^2}{R} \quad (36)$$

With V_{out_1} being the rms value of the first harmonic of the measured output voltage (18.3V) and R the load impedance at 34.5MHz, output power is experimentally estimated to 66.7W. Soft-switching is not perfectly attained

as shown in **Figure 16**. A possible way of improvement would be to adjust the value of C_p .

6 Conclusion and future work

This work has contributed to the production of a handful set of equations describing ideal operation of a FII class E inverter. This method allows exploration of design space, and an operating point can be chosen under specified constraints. A 100W 34.5MHz FII class E inverter has been designed and a prototype showing a good accordance with predicted performances has been presented. A complete process of modelling for VHF power converters, based on HF characterization and EM modelling, has been detailed. Forthcoming work is expected, and include:

- Shunt characterization of MLCC to better extract ESR and model the losses in capacitors
- Measure of output power and efficiency
- More integrated LC series filter with inductor printed on PCB. The output branch will be characterized and its impedance will be taken as an input to the analytical design.
- Design of a class E inverter more robust in front of load variations

7 Literature

- [1] Y. Wang, O. Lucia, Z. Zhang, Y. Guan, and D. Xu, 'Review of very high frequency power converters and related technologies', *IET Power Electron.*, vol. 13, no. 9, pp. 1711–1721, Jul. 2020,
- [2] A. Sarin, D. Abbot, S. Revzen, and A.-T. Avestruz, 'Bidirectional Capacitive Wireless Power Transfer for Energy Balancing in Modular Robots', in *2020 IEEE Applied Power Electronics Conference and Exposition (APEC)*, Mar. 2020, pp. 852–859.
- [3] J. Choi, D. Tsukiyama, Y. Tsuruda, and J. M. R. Davila, 'High-Frequency, High-Power Resonant Inverter With eGaN FET for Wireless Power Transfer', *IEEE Trans. Power Electron.*, vol. 33, no. 3, pp. 1890–1896, Mar. 2018,
- [4] M. P. Madsen, A. Knott, and M. A. E. Andersen, 'Very high frequency resonant DC/DC converters for LED lighting', in *2013 Twenty-Eighth Annual IEEE Applied Power Electronics Conference and Exposition (APEC)*, Mar. 2013, pp. 835–839.
- [5] J. Choi, Y. Ooue, N. Furukawa, and J. Rivas, 'Designing a 40.68 MHz power-combining resonant inverter with eGaN FETs for plasma generation', in *2018 IEEE Energy Conversion Congress and Exposition (ECCE)*, Sep. 2018, pp. 1322–1327.
- [6] W. Liang, L. Raymond, J. R. Davila, C. Charles, and R. Boswell, 'Structurally supportive RF power inverter for a CubeSat electrothermal plasma micro-thruster with PCB inductors', in *2017 IEEE Applied Power Electronics Conference and Exposition (APEC)*, Mar. 2017, pp. 2141–2145.
- [7] M. K. Kazimierczuk and D. Czarkowski, *Resonant power converters*, 2. ed. Hoboken, N.J: Wiley, 2011.
- [8] N. O. Sokal and A. D. Sokal, 'Class E-A new class of high-efficiency tuned single-ended switching

- power amplifiers', *IEEE J. Solid-State Circuits*, vol. 10, no. 3, Art. no. 3, Jun. 1975,
- [9] R. Zulinski and J. Steadman, 'Class E Power Amplifiers and Frequency Multipliers with finite DC-Feed Inductance', *IEEE Trans. Circuits Syst.*, vol. 34, no. 9, pp. 1074–1087, Sep. 1987,
- [10] M. Acar, A. J. Annema, and B. Nauta, 'Analytical Design Equations for Class-E Power Amplifiers', *IEEE Trans. Circuits Syst. Regul. Pap.*, vol. 54, no. 12, Art. no. 12, Dec. 2007,
- [11] I. Casallas, C.-I. Paez-Rueda, G. Perilla, M. Pérez, and A. Fajardo, 'Design Methodology of the Class-E Power Amplifier with Finite Feed Inductance—A Tutorial Approach', *Appl. Sci.*, vol. 10, no. 24, Art. no. 24, Jan. 2020,
- [12] S. Aldhafer, D. C. Yates, and P. D. Mitcheson, 'Load-Independent Class E/EF Inverters and Rectifiers for MHz-Switching Applications', *IEEE Trans. Power Electron.*, vol. 33, no. 10, Art. no. 10, Oct. 2018,
- [13] D. Reusch and J. Strydom, 'Evaluation of Gallium Nitride Transistors in High Frequency Resonant and Soft-Switching DC–DC Converters', *IEEE Trans. Power Electron.*, vol. 30, no. 9, pp. 5151–5158, Sep. 2015,
- [14] M. Beley, L. Pace, A. Bréard, and M. El-Khattabi, 'Caractérisation de deux gate drivers pour la commande de GaN-HEMT aux fréquences VHF', in *Symposium de Génie Electrique*, Lille, France, Jul. 2023.
- [15] L. Pace, N. Defrance, A. Videt, N. Idir, J.-C. De Jaeger, and V. Avramovic, 'Extraction of Packaged GaN Power Transistors Parasitics Using S-Parameters', *IEEE Trans. Electron Devices*, vol. 66, no. 6, pp. 2583–2588, Jun. 2019,

8 Appendix

The expressions of the coefficients presented in Section 2 and depending on q and D are given below.

Coefficients p and ϕ are either equal to (p_1, ϕ_1) or (p_2, ϕ_2) :

$$p_1 = \frac{\sqrt{(a_1c_2 - a_2c_1)^2 + (b_1c_2 - b_2c_1)^2}}{b_1a_2 - a_1b_2}$$

$$\phi_1 = \text{atan}(b_1c_2 - b_2c_1; a_1c_2 - a_2c_1)$$

$$p_2 = \frac{\sqrt{(a_1c_2 - a_2c_1)^2 + (b_1c_2 - b_2c_1)^2}}{-b_1a_2 + a_1b_2}$$

$$\phi_2 = \text{atan}(-b_1c_2 + b_2c_1; -a_2c_1 + a_1c_2)$$

Function $\text{atan}(y; x)$ gives the four-quadrant angle between $-\pi$ and $+\pi$ corresponding to parameters y and x .

With parameters a_1, a_2, b_1, b_2, c_1 and c_2 :

$$a_1 = \frac{q}{q^2 - 1} (\cos(2\pi q(D - 1)) - q^2 \cos(2\pi D)) + q$$

$$a_2 = \frac{q}{q^2 - 1} (\sin(2\pi q(D - 1)) - q \sin(2\pi D))$$

$$b_1 = \frac{q}{q^2 - 1} (-q \sin(2\pi q(D - 1)) + q^2 \sin(2\pi D))$$

$$b_2 = \frac{q}{q^2 - 1} (q \cos(2\pi q(D - 1)) - q \cos(2\pi D))$$

$$c_1 = 2\pi qD - \sin(2\pi q(D - 1))$$

$$c_2 = \cos(2\pi q(D - 1)) - 1$$

- Coefficients k_1 and k_2 :

$$k_1 = \frac{pq}{1 - q^2} (q \cos(2\pi q) \cos \phi + \sin(2\pi q) \sin \phi) - \cos(2\pi q)$$

$$k_2 = \frac{pq}{1 - q^2} (q \sin(2\pi q) \cos \phi - \cos(2\pi q) \sin \phi) - \sin(2\pi q)$$

Coefficient V_r for the FHA of voltage v_s :

$$V_r = \frac{V_{in}}{\pi} \left(\frac{k_1 r_1 + k_2 r_2 + p r_3}{q^2 - 1} + r_4 \right)$$

With parameters r_1, r_2, r_3 and r_4 :

$$r_1 = -\cos(2\pi qD) \cos(2\pi D + \phi) + \cos(2\pi q) \cos \phi \\ - q \sin(2\pi qD) \sin(2\pi D + \phi) \\ + q \sin(2\pi q) \sin \phi$$

$$r_2 = -\sin(2\pi qD) \cos(2\pi D + \phi) + \sin(2\pi q) \cos \phi \\ + q \cos(2\pi qD) \sin(2\pi D + \phi) \\ - q \cos(2\pi q) \sin \phi$$

$$r_3 = \frac{q^2}{4} (\cos(4\pi D + 2\phi) - \cos(2\phi))$$

$$r_4 = \cos(2\pi D + \phi) - \cos \phi$$

Coefficient V_x for the FHA of voltage v_s :

$$V_x = \frac{V_{in}}{\pi} \left(\frac{k_1 x_1 + k_2 x_2 + p x_3}{q^2 - 1} + x_4 \right)$$

With parameters r_1, r_2, r_3 and r_4 :

$$x_1 = \cos(2\pi qD) \sin(2\pi D + \phi) - \cos(2\pi q) \sin \phi \\ - q \sin(2\pi qD) \cos(2\pi D + \phi) \\ + q \sin(2\pi q) \cos \phi$$

$$x_2 = \sin(2\pi qD) \sin(2\pi D + \phi) - \sin(2\pi q) \sin \phi \\ + q \cos(2\pi qD) \cos(2\pi D + \phi) \\ - q \cos(2\pi q) \cos \phi$$

$$x_3 = \frac{q^2}{4} (4\pi(1 - D) - \sin(4\pi D + 2\phi) + \sin(2\phi))$$

$$x_4 = -\sin(2\pi D + \phi) + \sin \phi$$

- Coefficients for the RMS value of current i_s [11]:

$$f_1 = 0.4532 - 0.348q + 0.9159q^2 + 1.279D + 1.344D^2 \\ - 0.6721qD - 1.589q^2D^2 - 0.1598q^3 \\ + 0.7299D^3 + 1.039q^3D^3$$

$$f_2 = 3.615 - 7.482q + 3.686q^2 - 7.518D + 7.672D^2 \\ + 19.41qD - 11.87q^2D - 15.74qD^2 \\ + 9.707q^2D^2 + 0.1672q^3 - 0.6993D^3$$